JOURNAL OF OPTOELECTRONICS AND ADVANCED MATERIALS Vol. 10, No. 3, March 2008, p. 492 - 499

A simple synthesis and thermal decomposition kinetics of $MnHPO_4•H_2O$ rod-like microparticles obtained by spontaneous precipitation route

BANJONG BOONCHOM*, CHANAIPORN DANVIRUTAI[a]
King Mongkut's Institute of Technology, Ladkrabang Chumphon Campus, 17/1 M.6 Pha Thiew District, Chumphon, 86160, Thailand
[a]*Department of Chemistry, Faculty of Science, Khon Kaen University, Khon Kaen 40002, Thailand.*

Manganese hydrogenphosphate monohydrate ($MnHPO_4•H_2O$) was prepared by a rapid precipitation (10 min) using Mn(c)-H_3PO_4 system at ambient temperature. The thermal treatment of $MnHPO_4•H_2O$ at 773 K found to be a manganese pyrophosphate ($Mn_2P_2O_7$). The activation energies of the major mass loss step were calculated by Ozawa and Kissinger-Akahira-Sunose (KAS) isoconversional methods, which were used to determine the decomposition mechanism. The energy absorptions at the vibrational level of thermal decomposition steps were calculated and were compared with spectroscopic data, which were used to identify the molecules or ions that were released in each thermal transformation steps. The synthesized $MnHPO_4•H_2O$ and its thermal decomposition product $Mn_2P_2O_7$ were investigated by scanning electron microscope (SEM), X-ray powder diffraction (XRD) and Fourier transform infrared (FTIR) spectroscopy. The SEM micrographs show rod-like microparticles for the synthesized $MnHPO_4•H_2O$ and porosity on surface of the decomposition product $Mn_2P_2O_7$, which are important for specific applications.

(Received January 31, 2008; accepted March 12, 2008)

Keywords: Manganese hydrogenphosphate monohydrate, Rod-like microparticles, Porosity nanoparticles, Non-isothermal kinetics

1. Introduction

Manganese phosphates have recently raised more and more interest as materials to be used in the field of catalysts, laser host, magnetic and anti-proof corrosion [1-5]. Thermal treatment of manganese phosphates is a great synthetic potential, which relates to the hydrate in the conventional crystal form [6, 7]. They are transformed to other phosphates by hydrolysis and dehydration reactions at elevated temperatures [8-11]. Many of manganese phosphates are used as heterogeneous catalysts for a variety of organic processes [1-3]. There is a continuous academic and industrial interest in preparing new solid acid catalysts with different structures and acidity [4, 5]. Because of their acidity and porosity, layered materials represent a vast class of intercalating compounds with useful chemical and thermal properties, which have been extensively used as heterogeneous catalysts [12,13]. One representative of this material class, corresponding to the formula $MHPO_4•nH_2O$ (M= Zr, Mg, Mn and n=1-3) [7, 8], shows promise for applications in the field of ion exchange and catalysis [12].

$MnHPO_4•H_2O$ and $Mn_2P_2O_7$ have been used as catalysts and coating materials [12, 13]. However, a very little studies on synthesis and structure of $MnHPO_4•H_2O$ using manganese sulphate and phosphoric acid at pH 6, which SO_2 (g) was evolved [14]. Only the solubility and some thermodynamic properties of $MnHPO_4•H_2O$ were reported. Although $MnHPO_4•3H_2O$ was known earlier [15] by the reported crystal structure, which is isotypic with newberyite $MgHPO_4•3H_2O$ [16]. However, there is no data in the literature involving physical and chemical properties of $MnHPO_4•H_2O$. While $Mn_2P_2O_7$ has been prepared with thermal decomposition of $MnPO_4•H_2O$ [17], $Mn(H_2PO_4)_2•2H_2O$ [18] and $Mn_2P_2O_7•2H_2O$ [19]. The successful applications of the required material depend on the morphology and purity. The preparation of some metal phosphates by different synthesis conditions had been reported, giving to final metal phosphates with cost-effective methods [20]. However, these previously reported synthetic methods were time consuming and carried out high temperature, which are disadvantages of most general preparation methods are inhomogeneity, lack of soichiometry control and larger particle size.

Herein, the present paper reports the synthesis of $MnHPO_4•H_2O$ by spontaneous precipitation from manganese metal and 1 M H_3PO_4 at ambient temperature with the short time consuming (10 min) for the first time. Thermal treatment of the synthesized $MnHPO_4•H_2O$ at 773 K yielded as $Mn_2P_2O_7$, which is lower decomposition temperature than other manganese phosphates [17-19]. The thermal decomposition kinetic was carried out using the isoconversional methods of Ozawa [21] and Kissinger-Akahira-Sunose (KAS) [22]. A correlation between the temperature peak in DTA and the assigned wavenumbers are presented. This method reports a simple, rapid and cost effective route to synthesize rod-like microcrystalline of $MnHPO_4•H_2O$ and porous on surface of $Mn_2P_2O_7$. The porosity and particle sizes of $Mn_2P_2O_7$ are the reason of high catalytic activity, which remain a point of discussion

[12]. The prepared sample and its decomposition product were characterized by TG/DTG/DTA, XRD, SEM, and FTIR techniques.

2. Experimental

2.1 Sample preparation

The $MnHPO_4 \cdot H_2O$ compound was prepared by solution precipitation method using Mn (c; complexometric), 99.99 %, Merck) and phosphoric acid (86.4 %w/w H_3PO_4, Merck) as starting materials. In typical procedure, about 0.5 g of Mn (c) was dissolved in 5 mL of 1 M H_3PO_4. The resulting solution was stirred until $H_2(g)$ was completely evolved and the green gray precipitates were obtained (about 10 min). The prepared solid was filtered by suction pump, washed with water and dried in air.

2.2 Sample characterization

Thermal properties of $MnHPO_4 \cdot H_2O$ were investigated on a TG-DTA Pyris Diamond Perkin-Elmer Instruments in the temperature range of 303-1173 K. In accordance with TG-DTG/DTA results, the prepared sample was heated in a furnace at 773 K for 3 h and the dehydrated was obtained to be $Mn_2P_2O_7$. The manganese contents of $MnHPO_4 \cdot H_2O$ and $Mn_2P_2O_7$ compounds were determined by dissolving in 0.0126 M hydrochloric acid using atomic absorption spectrophotometry (AAS, Perkin Elmer, Analyst100). The phosphorus content was determined by colorimetric analysis of the molybdophosphate complex. The water content was analyzed by TG data. The structure and crystalline size of the prepared product as well as the calcined sample were studied by X-ray powder diffraction using a D8 Advanced powder diffractometer (Bruker AXS, Karlsruhe, Germany) with Cu Kα radiation (λ = 0.1546 nm). The Scherrer method was used to evaluate the crystalline size (i.e. $D = K\lambda/\beta\cos\theta$, where λ is the wavelength of X-ray radiation, K is a constant taken as 0.89, θ is the diffraction angle and β is the full width at half maximum (FWHM)) [23]. The morphologies of the prepared sample and of its decomposition product were examined with scanning electron microscope using LEO SEM VP1450 after gold coating. The room temperature FTIR spectra were recorded in the range of 4000-370 cm^{-1} with 8 scans on a Perkin-Elmer Spectrum GX FT-IR/FT-Raman spectrometer with the resolution of 4 cm^{-1} using KBr pellets (spectroscopy grade, Merck).

2.3 Activation energy by isoconversional method

To evaluate the activation energies for the thermal decomposition of $MnHPO_4 \cdot H_2O$, a TG-DTA Pyris Diamond Perkin-Elmer Instrument was used. The experiments were performed in static air, at heating rates of 5, 10, 15, and 20 K min^{-1} over the temperature range from 303 to 773 K and the O_2 flow rate of 100 mL min^{-1}. The sample mass of about 6.0-10.0 mg was filled into alumina crucible without pressing. The thermogram of sample was recorded in an open aluminum pan using α-Al_2O_3 as the reference material. Dehydration of crystal hydrates is a solid-state process of the type [24-27]: A(solid) →B (solid) + C (gas). The kinetics of such reactions is described by various equations taking into account the special features of their mechanisms. This is a model-free method, which involves measuring the temperatures corresponding to fixed values of α (extent of conversion) from experiments at different heating rates (β). The activation energy (E_α) can be calculated according to the isoconventional methods. In kinetic study of $MnHPO_4 \cdot H_2O$, Ozawa [21] and KAS [22] equations were used to determine the activation energy of the decomposition reaction.

The equations used for E_α calculation are:

Ozawa equation:

$$\log\beta = \log\left(\frac{AE_\alpha}{R\,g(\alpha)}\right) - 2.315 - 0.4567\left(\frac{E_\alpha}{RT}\right) \quad (1)$$

KAS equation:

$$\ln\left(\frac{\beta}{T^2}\right) = \ln\left(\frac{AE_\alpha}{R\,g(\alpha)}\right) - \left(\frac{E_\alpha}{RT}\right) \quad (2)$$

where A (the pre-exponential factor) and E (the activation energy) are the Arrhenius parameters and R is the gas constant (8.314 J $mol^{-1} \cdot K^{-1}$). The Arrhenius parameters, together with the reaction model, are sometimes called the kinetic triplet. $g(\alpha) = \int_0^\alpha \frac{d\alpha}{f(\alpha)}$ is the integral form of the $f(\alpha)$, which is the reaction model that depends on the reaction mechanism.

According to isoconversional method, the basic data of α and T were collected from the TG curves for the major mass loss of $MnHPO_4 \cdot H_2O$ in air at various heating rates (5, 10, 15 and 20 K min^{-1}). According to the equations 1 and 2, the plots of log β versus 1000/T (Ozawa) and ln β/T^2 versus 1000/T (KAS) corresponding to different conversions α can be obtained by a linear regress of least-square method, respectively. The activation energies E_α can be calculated from the slopes of the straight lines with better linear correlation coefficient (r^2).

3. Results and discussion

3.1 Thermal analysis

The TG-DTG-DTA curves of $MnHPO_4 \cdot H_2O$ are shown in Fig.1. The TG curve shows the weight loss between 303 and 1073 K, which is related to the elimination of water molecules and the changing of phase

transformations. The eliminations are observed in two areas: 403-593 and 593-693 K, which correspond to weight losses of 10.11 and 6.89 % by mass and 0.94 and 0.64 mol of water, respectively. Three endothermic effects over the temperature region are observed in DTA curve at 470, 521 and 611 K, where appear peaks in DTG curve. Further, a small exothermic effect at 844 K without appreciable weight loss is observed in the DTA curve, which can be ascribed to a transition phase from amorphous to crystalline form of $Mn_2P_2O_7$. The thermal decomposition of $MnHPO_4•H_2O$ involves the dehydration of the coordinated water molecule (1 mol H_2O) and an intramolecular dehydration of the protonated phosphate groups (0.5 mol H_2O), these processes formally could be presented as:

$$MnHPO_4•H_2O \longrightarrow MnHPO_4 + H_2O \quad (3)$$

$$MnHPO_4 \longrightarrow 1/2Mn_2P_2O_7 + 1/2H_2O \quad (4)$$

Subsequently it has been shown that the water of crystallization cannot be usually removed without the destruction of anion structure, because the first step of the scheme given above are often overlapped. This reason confirms two peaks in DTG and DTA curves. Manganese pyrophosphate, $Mn_2P_2O_7$ is found to be the final product of the thermal decomposition at T > 673 K. Total mass loss is 17.00 % (1.58 mol H_2O) which is close to theoretical value (16.17 %, 1.50 mol H_2O). In order to gain the complete dehydration of $MnHPO_4•H_2O$, the sample of $MnHPO_4•H_2O$ was heated in the furnace at 773 K for 3 h and the decomposition product as $Mn_2P_2O_7$ was obtained at lower temperature and shorter time than that of the production by the other precursors and preparation methods (e.g. $MnPO_4•H_2O$ at 873 K [17], $Mn(H_2PO_4)_2•2H_2O$ at 1073 K [18], $Mn_2P_2O_7•2H_2O$ at 973 K [19], $Mn_2P_2O_7$ at > 873 K [28]).

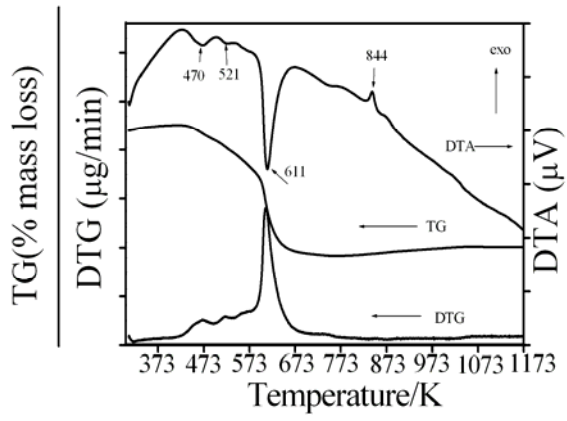

Fig. 1. TG-DTG-DTA curves of $MnHPO_4•H_2O$ in air at four heating rates (10 $Kmin^{-1}$).

.

The specificity of the thermal decomposition was characterized by identification of the bonds to be selectively activated due to energy absorption at vibrational level [29]. These bonds were assigned by comparing the calculated wavenumbers with the observed wavenumbers in the IR spectra. This breaking bond is assimilated with a Morse oscillators [29] coupled non-linear [30] with the harmonic oscillators of the thermic field. Following, a theoretical treatment developed by Vlase et al.[24], this work applies the relation between the maximum temperature peak T_p (DTA) at heating rate of 10 K min^{-1} and the wavenumber of activated bond is calculated by:

$$\omega = \frac{k_b}{hc} T_P = 0.695 T_p \quad (5)$$

where k_b and h are respectively the Boltzmann and Planck constants, and c the light velocity. Because the breaking bond has an unharmonic behavior, the specific activation is possible due to more than one quanta, or by a higher harmonic. Here, ω_{cal} is calculated by Eq.(5), which is assigned the spectroscopic number for the bond supposed to break. ω_{sp} are the frequency bands of vibrational modes and are calculated by $\omega_{sp} = q\omega_{calc}$, $q \in N$ =1,2,3,…, (quanta number). Additionally, the ω_{cal} values with the ω_{sp} values determined from the DTA, together with the assignments of the corresponding oscillations are compared. In this paper we suggested the maximum temperature peak T_p in DTA curve for the calculated wavenumbes (ω_{sp}) according to Eq. (5). In order to corroborate the calculated data with the spectroscopic ones, we drew up the FT-IR spectra of the studied compound (Fig. 6). Three T_p peaks at heating rate of 10 K min^{-1} in DTA curve are observed at 470, 521 and 611 K. The correlated harmonic energy (ω_{calc}) values calculated from three T_p peaks are 1633 (q=5), 3267 (10), 3594 (11) cm^{-1} and 724 (2), 1086 (3), 2897 (8) cm^{-1} and 849 (2), 1273 (3), 1698 (4), 3397 (8) cm^{-1}, respectively. These results show the elimination of water of crystallization (the first step), followed by a continuous intermolecular polycondensation and elimination of water of the hydrogenphosphate groups (the second step) [27], whereas the third step indicates the overlapping of the elimination of water of crystallization and the destruction of HPO_4^{2-} anion structure. The studied compound exhibited a very good agreement between the calculated wavenumbers from average T_p (DTA) and the observed wavenumbers from IR spectra for the bonds suggested being broken. These results indicate the use of T_p (DTA) will be an alternative method for the calculated wave numbers for identification of each thermal transition step of interesting materials.

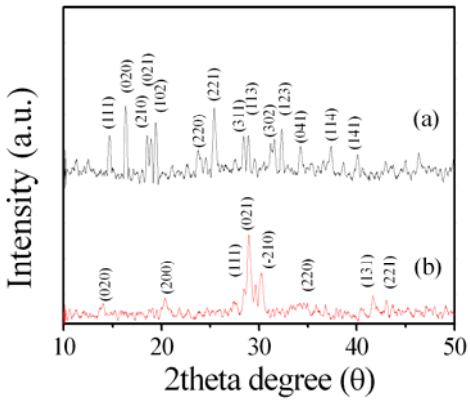

Fig. 2 XRD patterns of $MnHPO_4•H_2O$ (a) and its decomposition product $Mn_2P_2O_7$ (b).

3.2 X-ray powder diffraction

The XRD patterns of $MnHPO_4• H_2O$ and its decomposition product $Mn_2P_2O_7$ are shown in Fig. 2. The XRD pattern of $MnHPO_4• H_2O$ is similar to that of $MnHPO_4•3H_2O$, which are the same material class of the formula $Mn(HPO_4)_2•nH_2O$ (n=1-3) [6, 7] due to their isostructural. All detectable peaks are indexed as $MnHPO_4•H_2O$ and $Mn_2P_2O_7$ with structure comparable to the standard data as PDF # 250541 ($MnHPO_4•3H_2O$) and PDF # 771243 ($Mn_2P_2O_7$), respectively. These results indicated that $MnHPO_4•H_2O$ crystal structure is in orthorhombic system with space group Pbca (Z = 8) and $Mn_2P_2O_7$ crystal structure is in monoclinic system with space group C2/m (Z = 4). The average crystallite sizes and lattice parameters of $MnHPO_4•H_2O$ and $Mn_2P_2O_7$ were calculated from X-ray spectra and tabulated in Table 1. The lattice parameters of $MnHPO_4•H_2O$ and $Mn_2P_2O_7$ are comparable to those of the standard data as PDF # 250541 ($MnHPO_4•3H_2O$) and PDF # 771243 ($Mn_2P_2O_7$), respectively. The crystallite size of $MnHPO_4•H_2O$ is larger than that of $Mn_2P_2O_7$, which is the effect of the dehydration processes. The crystallite size of 27 ± 12 nm for $Mn_2P_2O_7$ in this work is smaller than that of the calcined $MnPO_4• H_2O$ precursor at 873 K (54 ± 18 nm) [17] and $Mn(H_2PO_4)_2 • 2H_2O$ at 1073 K (36 ± 8 nm) in our previous study [18]. The XRD results confirm that the differences in the crystallite sizes for the synthesized $Mn_2P_2O_7$ depend on the thermal decomposition of precursors and conditions for precipitation.

Table 1. Average crystallite sizes and lattice parameters of $MnHPO_4•H_2O$ and $Mn_2P_2O_7$ calculated from XRD data.

Compounds	Systems	a (Å)	b (Å)	c (Å)	β (°)	Average crystallite size (nm)
$MnHPO_4•3H_2O$	PDF#25-0541	10.44	10.87	10.22	-	-
	This work	10.45 (1)	10.75 (0)	10.18(0)	-	39 ± 9
DIF. This work -PDF		+0.01	-0.12	-0.04	-	
$Mn_2P_2O_7$	PDF#77-1243	6.633	8.583	4.646	102.67	-
	This work	6.546(0)	8.438(0)	4.616(0)	102.88(1)	27 ± 12
DIF. This work -PDF		-0.087	-0.145	-0.030	+0.21	

3.3 Scanning electron microscopy

The changing morphology of $MnHPO_4• H_2O$ and its decomposition product $Mn_2P_2O_7$ are shown in Fig. 3. The particle shape and size are changed throughout the whole decomposition product. The SEM micrograph of $MnHPO_4• H_2O$ (Fig. 3a) illustrates many small and some large rod-like particles, having sizes of about 0 .20– 1.00 μm in length and 0.10–0.50 μm in width for small rod-like crystals and about 0 .40– 3.00 μm in length and 0.40–1.50 μm in width for large rod-like crystals, respectively. The calcined $Mn_2P_2O_7$ shows re-texturing and coalescence in aggregates of nonuniform crystals of different sizes and a porous structure appearing on its surface (Fig. 3b), which is similar to that of $Mn_2P_2O_7$ [17, 18]. However, the present sample in this work has larger particle sizes and porosity than that of the reported previously work [17, 18]. The SEM micrographs indicate that thermal decomposition of different precursors have the strong effect on the morphology of $Mn_2P_2O_7$. The particle size and porosity of $MnHPO_4• H_2O$ and $Mn_2P_2O_7$ are the reason of high catalytic activity, which remain a point of interest not yet completely understood. The SEM experiment results indicate that the particle sizes of $MnHPO_4• H_2O$ are smaller than that of its decomposition product $Mn_2P_2O_7$, those are in consistent with the results of XRD analysis.

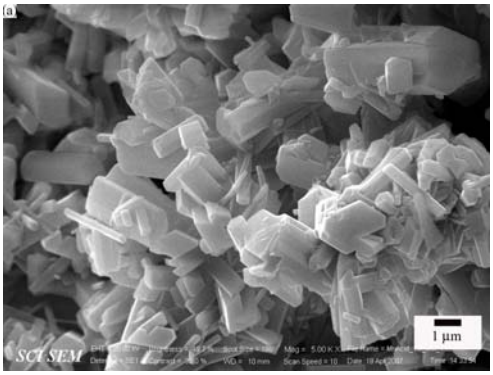

Fig. 3 SEM micrographs of $MnHPO_4$•H_2O (a) and its decomposition product $Mn_2P_2O_7$ (b).

3.4 FTIR spectroscopy

The FT-IR spectrum of $MnHPO_4$• H_2O is very similar to that observed by Šoptrajanova et al. [31], which are assigned relative to the fundamental vibrating units, HPO_4^{2-} and H_2O (Fig. 4). The highest site symmetry of HPO_4^{2-} ion is C_{3v}, in the crystallographic unit cell (Pbca, Z = 8) [15], however, the eight HPO_4^{2-} ions are located on the set of non-equivalent site symmetry of C_1. A pair of HPO_4^{2-} ions is related to each other by a center of symmetry. The free PO_4^{3-} ion has four normal modes of vibration of a tetrahedral ion. They are ν_1 (A_1) symmetric stretching; ν_3 (F_2) asymmetric stretching; and ν_4 (F_2) and ν_2 (E) bending vibrations [31, 32]. All four modes are Raman active, whereas only ν_3 (asymmetric stretching) and ν_4 (the out-of plane bending) are IR active. The ν_3 and ν_4 modes are triply degenerate, ν_2 is doubly degenerate and ν_1 is non-degenerate. The four fundamental modes of the free phosphate ion undergo factor group splitting [31], which indicate the symmetry reduction of the PO_4^{3-} (T_d) units in the structure. The fact that the symmetric stretching mode is observed in the infrared spectrum affirms a reduction in symmetry of the PO_4^{3-} units. As expected for a rather strongly H-bonded hydrogenphosphate, the anion O–H stretchings give rise to a complex infrared feature (A, B, C trio [31]) of which two components (centered around 2800 and 2400 cm^{-1}) are clearly visible (Fig. 4), the third component (C) possibly contributing to the breath of the bands in the water bending region (1850-1495 cm^{-1}) and/or the multiple bands in this region. The B band seems to be the stronger, but the A and C bands are difficult to observe accurately, because the strong H_2O absorption appears in the same spectral range. The O–H stretching (B band) wavenumber of HPO_4^{2-} ions is estimated about 2350-2450 cm^{-1}, which indicate the stronger hydrogen bond in this compound. Consequently, the acidity of $MnHPO_4$• H_2O as the reason of high catalytic activity remains a point of contentions. The intense band at about 1236 cm^{-1} is due to the in-plane P-O-H bending (A_2), while the out-of-plane bending (A_1) vibration is observed at about 885 cm^{-1}. Vibrational spectra of present hydrate were assigned by factor group analysis and derived from the same mode in the free HPO_4^{2-} ion [31, 32]. A strong band at about 1148 cm^{-1} in FTIR spectra is assigned to PO_3 asymmetric stretching (B_1), while the other one at about 1050 cm^{-1} correspond to PO_3 symmetric stretching modes (E). The FTIR frequency of the PO_3 symmetric stretching (A_1) shows the strong band at about 998 cm^{-1}. The weak and broader band at about 885 cm^{-1} is assigned to P-OH symmetric stretching modes (A_1). The medium band at about 547, 523 and 505 cm^{-1} are corresponding to PO_4 (E) and P-OH (A_1) bending modes.

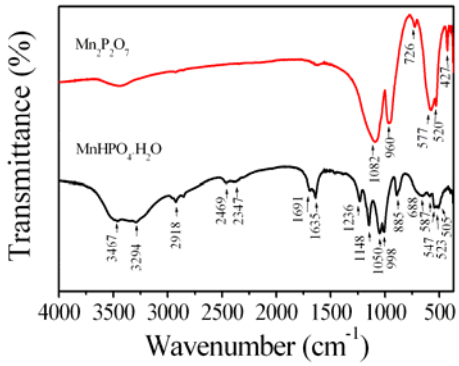

Fig. 4 FT-IR spectra of $MnHPO_4$•H_2O and its decomposition product $Mn_2P_2O_7$.

Unlike the $H_2PO_4^-$ ion, one water molecule occupies a general position in the crystal [31]. The band of water vibrations are illustrated in Fig. 4 as a doublet bands (1691 and 1635 cm^{-1}) contributes both to the C band and to the water bending region ((ν_2; A_1) [31-33]. A weak band occurs in the FTIR spectra at approximately 688 cm^{-1} is assigned to rocking librational mode of water molecules. The ν_{OH} stretching modes of HOH in MnH_2PO_4 •H_2O are observed at 3467 cm^{-1} (ν_3; B_2) and 3294 cm^{-1} (ν_1; A_1).

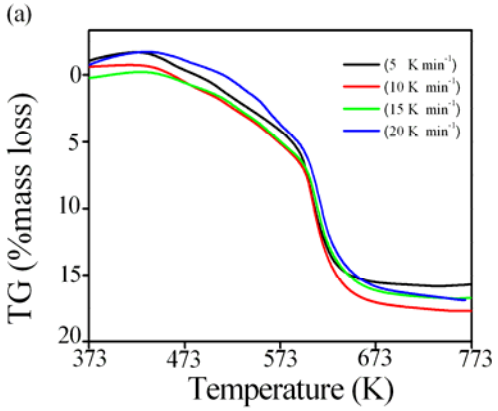

Fig. 5. TG (a)-DTG (b)-DTA (c) curves of $MnHPO_4$•H_2O in air at four heating rates (5, 10, 15 and 20 $Kmin^{-1}$).

The FTIR spectrum of the $MnHPO_4•H_2O$ calcined at 773 K (Fig.4) is similar to that of $Mn_2P_2O_7$ [34-36]. It has been reported that the degree of multiplication and fineness in the spectra of phosphates increase as the degree of polymerization increases in the tetrahedral $[PO_4]$. It is clearly noticed that the studied compounds exhibit more splitting and sharpness, especially in the low-frequency regions, indicating polymerization of $[PO_4]^{3-}$ to $[P_2O_7]^{4-}$. The strong vibrational band at 1086 cm^{-1} is attributed to the stretching of PO_3 units. The asymmetric (ν_{asym} POP) and symmetric stretch (ν_{sym} POP) bridge vibrations for this sample are observed at about 960 and 726 cm^{-1}, while he asymmetric (δ_{asym} PO_3) and symmetric (δ_{sym} PO_3) bending vibrations are observed at about 577 and 520 cm^{-1}, respectively. The PO_3 deformation, rocking modes, the POP deformations, the torsional and external modes are found in the 400–230 cm^{-1} region.

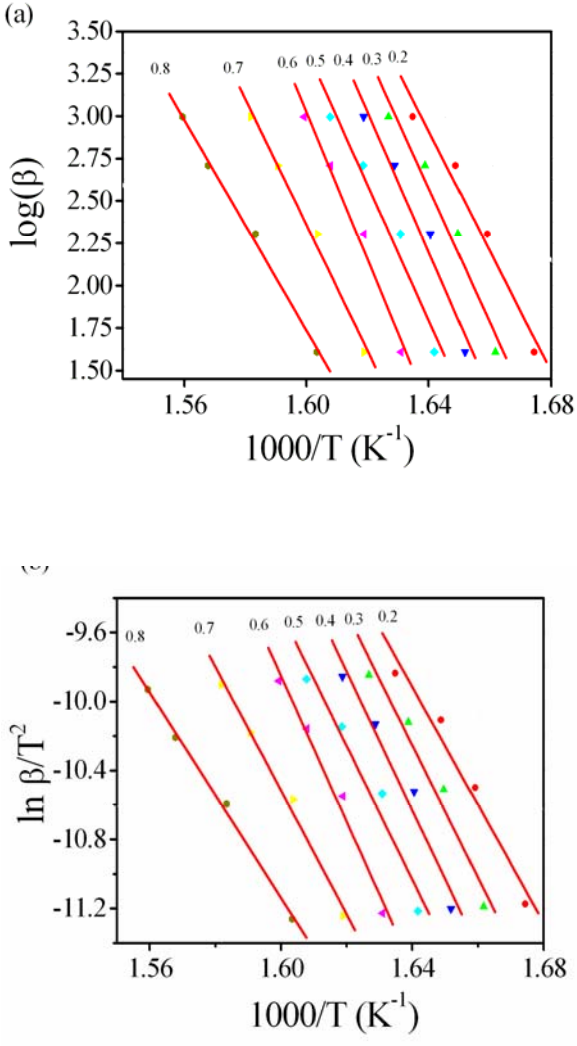

Fig.6. Ozawa (a) and KAS (b) analysis of four TG measurements for the first step.

3.5 The calculation of activation energy

Non-isothermal TG method is desirable to analyze the reaction mechanism and calculate the activation energy of the solid state [24-27]. The TG results (Fig 5) were further subjected to kinetic analyses in order to find out the activation energy values. Several non-isothermal techniques have been proposed which are quicker and less sensitive to previous and next transformations. In addition, they can provide the more accurate activation energy and crystal growth mode. Kinetics analysis shows only major mass loss in the region of 593-693 K for the decomposition of $MnHPO_4•H_2O$. Because the other steps are minor mass loss in the short temperature ranges, they are highly sensitive to non- isothermal kinetics analysis errors. According to the equations (1) and (2), the slopes change depending on the degree of conversion (α) for the decomposition reaction (Fig. 6). E_α ($0.8<\alpha<0.2$) values calculated from Ozawa and KAS isoconversional methods on the obtained data of the TG curves are illustrated in Table 2. It was considered that the E_α value is heating rate independent if the relative error of the slope of Ozawa and KAS straight lines is lower than 10 %. For this step, E_α values calculated by Ozawa method in the α range of 0.2-0.8 are close to those of obtained by KAS method. If neglecting the dependence of E vs.α, an average values of E = 302.31± 32 kJ mol^{-1} (Ozawa) and 307.66± 34 kJ mol^{-1} (KAS), are obtained. The activation energy for the losing of water crystallization lie in the range of 60–130 kJ mol^{-1}, while the value for coordinately bounded one are higher this range [37]. The calculated higher activation energies for the dehydration reaction of this compound (Table 2) suggest that the water molecules are coordinated water, which indicate the strong overlapped of the different water molecules in this structure. From considering the dependence of E vs. α, a strong dependence of the activation energy on the α are obtained. If E_α values vary with α, the dehydration may be a simple reaction [38], whereas the dependence of E on α should be interpreted in terms of multi-step reaction mechanisms [24]. Therefore, we draw the conclusion that the decomposition of $MnHPO_4•H_2O$ may be multi-step reaction mechanisms, which correspond to the overlapped breaking bond of O-H (HOH) and a true P-OH in connection with polycondensation reaction. This result confirms that the decomposition product $Mn_2P_2O_7$ was obtained. Additionally, E_α values decrease or increase with α confirming the different strengths of binding of water molecules in crystal lattice, which are affected by strong overlapped in this step. The strengths of the molecular binding in the crystal lattice are different. Consequently, the dehydration temperatures are different. The dehydration temperatures and the calculated activation energy obtained in this work suggest that the water in $MnHPO_4•H_2O$ can be considered as coordinated water [37], which is consistent with TG/DTG/DTA data and the calculated activation energies from FWO and KAS methods.

Table 2. Activation energies E_α and correlation coefficient (r^2) calculated by FWO and KAS methods for the dehydration step of $MnHPO_4 \bullet H_2O$ (453 – 523 K).

α		FWO method			KAS method	
		E_α/kJ mol^{-1}	r^2		E_α/kJ mol^{-1}	r^2
0.2		280.07	0.98459		284.48	0.98349
0.3		312.83	0.98141		318.86	0.98023
0.4		326.23	0.98367		332.89	0.98267
0.5		315.60	0.97983		321.65	0.97855
0.6		342.96	0.99139		350.36	0.99087
0.7		293.18	0.99523		297.92	0.99489
0.8		245.31	0.99823		247.46	0.99807
Average		302.31± 32	0.9878		307.66± 34	0.9870

4. Conclusion

The $MnHPO_4 \bullet H_2O$ sample was obtained by a simple spontaneous precipitation from Mn(c) and 1 M H_3PO_4 at ambient temperature with short time consuming (10 min). The thermal transformation product at 773 K is manganese polyphosphate ($Mn_2P_2O_7$). The transformation temperature is lower than that of the calcined product of the other precursors. The XRD and FTIR spectra confirm the formation of $MnHPO_4 \bullet H_2O$ and $Mn_2P_2O_7$ compounds. The morphologies of $MnHPO_4 \bullet H_2O$ and its thermal transformation products show rod-like micropaticles and porosity on its surface, respectively. Thermal kinetic study results indicate the activation energies relate to vibrational frequencies of breaking bond of thermal transformation of $MnHPO_4 \bullet H_2O$. The major mass loss step relates a multi-step reaction mechanism, which confirms the strong overlapping according to the bond breaking energies of the intermediate species. This work presents the simple, cost effective and short time consuming method for the preparation of $MnHPO_4 \bullet H_2O$ and $Mn_2P_2O_7$ compounds. Both compounds have many interesting potential applications including catalytic, ceramic and magnetic materials.

Acknowledgements

The authors would like to thank the Chemistry Department, Khon Kaen University for providing research facilities. This work is financially supported by King Mongkut's Institute of Technology Ladkrabang (KMITL), Ministry of Education, Thailand.

References

[1] A. Jouini, J.C. Gâcon, M. Ferid, M. Trabelsi-Ayadi, Opt. Mater. **24,** 175 (2003).
[2] T. Kitsugi, T. Yamamuro, T. Nakamura, M. Oka, Biomaterials. **16,** 1101 (1995).
[3] B. Jian-Jiang, K. Dong-Wan, H. Kug Sun, J. Eur. Ceram. Soc. **23,** 2589 (2003).
[4] J. R. Martinelli, F. F. Sene, L. Gomes, J. Non-Cryst. Solids. **263,** 299 (2000).
[5] P. Carmen, P. Josefina, S.P. Regino, R.V. Caridad, S. Natalia, Chem. Mater. **15,** 3347 (2003).
[6] Ž. Mesíková, P. Šulcová, M. Trojan, J. Therm. Anal. Cal. **88,** 103 (2007).
[7] A. Bensalem, G. Iyer, J. Solid State Chem. **114,** 598 (1995).
[8] H. Onoda, K. Kojima , H. Nariai, J. Alloys Comp. **408–412,** 568 (2006).
[9] H. Onoda, H. Nariai, H. Maki, I. Motooka, Mater. Chem. Phys. **73** (1)**,**19 (2002).
[10] H. Onoda, A. Takenaka, K. Kojima, H. Nariai, Mater. Chem. Phys. **82** (1), 194 (2003)
[11] M. A. Aramendía, V. Borau, C. Jiménez, J. M. Marinas, F. J. Romero, J. Colloid Interface Sci. **217**, 288 (1999).
[12] S.M. Al-Zahrani, N.O. Elbashir , A.E. Abasaeed, M. Abdulwahed, Catal. Lett. **69**,65 (2000).
[13] H.Assaaoudi, I.S.Butler, J.A. Kozinski. J. Chem. Cryst. **36,** 723 (2006).
[14] P.P. Maharatra, A.K. Dash, N.S. Chickerur. Thermochem. Acta. **70,** 163 (1983).
[15] Y. Cudennec, A. Riou, Y. Geraut, Acta Crystallogr. **C45**, 1411 (1989).

[16] B. C. Sales, B. C. Chakoumakos, L. A. Boatner, J. O. Ramey. J. Non-Cryst. Solids **159**, 121 (1993).
[17] B. Boonchom, S. Youngme, S. Maensiri, C. Danvirutai. J. Alloys Compd. (2006) (in press). (doi:10.1016/j.jallcom.2006.12.064).
[18] B. Boonchom, C. Danvirutai, S. Maensiri, Mater. Chem. Phys. xxx (2008) xxx.
[19] S. Schneider, R.L. Collin. Inorg. Chem. **12**, 2136 (1973).
[20] A. Manthiram, J. Kim, Chem. Matter. **10**, 2895 (1998).
[21] T. Ozawa, T. Bull. Chem. Soc. Jpn. **38**, 1881 (1965).
[22] H.E. Kissinger. Anal. Chem. **29**, 1702 (1957).
[23] B.D. Cullity, Elements of X-ray Diffraction, second ed., Addison-Wesley Publishing, 1977.
[24] T. Vlase, G. Vlase, M. Doca, N. Doca, J. Therm. Anal. Cal. **72**, 597 (2003).
[25] Y. Zhang, M. Lv, D. Chem, J. Wu, Mat. Lett. **61**, 2978 (2007).
[26] T. Vlase, G. Jurca, N, Doca, Thermochim. Acta. **379,** 65 (2001).
[27] A. Ioițescu, G. Vlase, T.Vlase, N. Doca, J. Therm. Anal. Cal. **88**, 121 (2007).
[28] K. Benkhouja, M. Zahir, A. Sadel, A. Handizi, A. Boukhari, E. M. Holt, J. Aride, M. Drillon. Mater. Res. Bull. **30**, 49 (1995).
[29] G. Herzberg, Molekülspektren und Molekülstruktur I. Zweiatomige Moleküle, Steinkopff, Dresden 1939.
[30] N. B. Colthup, L. H.Daly, S.E. Wiberley, "Introduction to Infrared and Raman Spectroscopy" Academic Press, New York 1964.
[31] B. Šoptrajanov, V. Stefov, I. Kuzmanovski, G. Jovanovski. J. Mol. Struct. **482**–**483**, 103 (1999).
[32] J.R. Ferraro, J.S. Ziomek. Introductory Group Theory and Its Application to Molecular Structure, Plenum Press, New York (1975).
[33] B. J. M. Rajkumar, V. Ramakrishnan. Spectrochim. Acta. **57A**, 247 (2001).
[34] E. Steger, B. Käßner, Spec trochim. Acta. **24A**, 447 (1968).
[35] E. H. Soumhi, I. Saadoune, A. Driss. J. Solid State Chem. **156** 364 (2001).
[36] A. C. Chapman, Spectrochim. Acta. **24A**, 1678 (1968).
[37] M. A. Gabal, Thermochim. Acta. **402,** 199 (2003).
[38] S. Vyazovkin, Int. J. Rev. Phys. Chem. **19,** 45 (2000).

*Corresponding author: chanai@kku.ac.th, kbbanjon@kmitl.ac.th